Experimental Validation Study of 3D Direct Simple Shear DEM Simulations

Michelle L. Bernhardt[a,*], Giovanna Biscontin[b], and Catherine O'Sullivan[c]

[a]Department of Civil Engineering, University of Arkansas, Arkansas, USA
[b]Department of Engineering, Cambridge University, Cambridge, UK
[c]Department of Civil and Environmental Engineering, Imperial College London, London, UK

Abstract

Simple shear element tests can be used to examine numerous geotechnical problems; however, the cylindrical sample (NGI-type) direct simple shear (DSS) devices have been criticized for an inability to apply uniform stresses and strains, as well as the inability to fully define the stress state of the soil during shearing. Discrete element method (DEM) simulations offer researchers a means to explore the fundamental mechanisms driving the overall behavior of granular soil in simple shear, as well as improve understanding of the DSS device itself. Here three-dimensional DEM simulations of laminar NGI-type direct simple shear element tests and equivalent physical tests are compared to validate the numerical model. This study examines the sensitivity of the DEM simulation results to sample size, contact model and stiffness inputs, and ring wall boundary effects. Sample inhomogeneities are also considered by examining radial and vertical void ratio distributions throughout the sample. Both the physical experiments and the DEM simulations presented indicate that the observed material response is highly sensitive to the particle size relative to the sample dimensions. The results show that samples with a small number of relatively large particles are very sensitive to small changes in packing, and thus an exact match with the DEM simulation data cannot be expected. While increasing the number of particles greatly improved the agreement of the volumetric and stress-strain responses, the dense DEM samples are still initially much stiffer than the experimental results. This is most likely due to

the fact that the inter-particle friction was artificially lowered during sample preparation for the DEM simulations to increase the sample density.

1. Introduction and background

Simple shear element tests are used to study soil behavior for a number of geotechnical problems including: foundation loading, traffic/pavement loading, pile driving, slope stability, and earthquakes (Bjerrum and Landva, 1966; Randolph and Wroth, 1981; Malek, 1987). Simple shear devices aim to recreate the in situ stress state and mode of deformation for an element of soil by applying an approximately uniform shear strain field to the sample and allowing the principal axes to smoothly rotate, a feature which is not possible in triaxial testing. The two types of experimental devices commonly used to study deformation in simple shear are the direct simple shear (DSS) device, consisting of either a cylindrical or parallelepiped sample, and the torsional shear hollow cylinder apparatus (HCA) which uses a hollow cylindrical sample. The advantages and disadvantages of these devices have been outlined by several researchers (Sada et al., 1983; Shibuya and Hight, 1987; Talesnick and Frydman, 1991). The advantage of the HCA is that it allows for all three principal stresses to be directly measured and, theoretically, independently controlled, however sample preparation is difficult. While sample preparation and testing in the cylindrical sample DSS device, often referred to as the NGI-type device for developments made at the Norwegian Geotechnical Institute (Bjerrum and Landva, 1966), is relatively simple, several limitations have hindered its widespread acceptance (Saada and Townsend, 1981; LaRochelle, 1981; Airey et al., 1985; Talesnick and Frydman, 1991; Jardine and Menkiti, 1999).

DSS devices are not able to apply the complementary shear stresses present in the ideal simple shear case, which leads to non-uniformities across the top and bottom

boundaries. While this violates ideal simple shear conditions, Franke et al. (1979) and Vucetic (1981) showed that these non-uniformities are minimized for large diameter to height ratios. Budhu and Britto (1987) also showed that the sample core is under ideal simple shear conditions. An additional limitation of the NGI-type device is the difficulty of measuring the horizontal normal stress during shearing and the fact that it does not correspond to the intermediate principal stress or the stress normal to the plane perpendicular to shearing (Budhu, 1988). These factors lead to an incomplete description of the changing stress state of the soil and require several assumptions to be made regarding the failure mechanisms in order for the strength parameters to be assessed. There is a need to examine the stresses and strains within the soil element and determine the microscopic interactions driving the overall behavior.

Several researchers have used numerical methods to study DSS element tests in an effort to better understand the stress state and the strain distributions. Finite element analyses were performed by Budhu and Britto (1987), Dounias and Potts (1993), Bashir and Goddard (1991), and Zhuang (1993). While they provide insight into the mechanism of simple shear, FEM models are limited in their ability to capture the full and complex nature of granular materials and their interactions at the particulate scale. Others have used discrete element method (DEM) simulations which naturally allow granular behavior to arise through the use of very simple contact models and without the need for a complex constitutive material law (Shen, 2013; Dabeet et al., 2011; Ai et al., 2014). These studies demonstrated that DEM simulations are particularly advantageous for studying element tests on granular soils because they allow examination of particle-scale interactions, localized measurements of stresses and strains, and quantitative analysis of fabric.

The documented direct simple shear DEM studies differ mainly in their treatment of the boundary conditions. In a two-dimensional DEM study, Shen et al. (2011) considered

both the hinged rigid walls in the parallelepiped sample Cambridge device, and laminar walls which simulate the stack of lateral confining rings often used in the NGI-type device. Shen et al. showed that the type of boundary walls used influences the microscopic response observed, even though the macroscopic response was similar. This indicates the importance of modeling the correct boundary conditions if simulations of element tests are to be useful to examining micro-scale behavior. Ai et al. (2014) conducted a two-dimensional DEM simple shear study on non-coaxial granular behavior using a discretized wall system to limit the boundary non-uniformities imposed on the element. While these two-dimensional studies captured much of the behavior observed in granular materials in simple shear, they were not able to examine the three-dimensional response and out of plane displacements which are present in real granular materials.

In the only documented three-dimensional study, Dabeet et al. (2011) used laboratory data for glass beads to calibrate direct simple shear simulations. The stress strain curves from simulations with various linear stiffness values were compared to experimental data to calibrate the model. The DEM model considered a single rigid cylindrical-walled sample to represent the NGI-type device used in the laboratory. While this approach is computationally efficient, it is unclear if the rigid wall in this three-dimensional simulation affects the microscopic results as it does in the two-dimensional case.

If DEM simulations of simple shear element tests are to provide useful insight into the device, it is important that they are properly validated by experimental data. Validation studies consist of developing DEM models which replicate the physical conditions as accurately as possible. The size, number, and material properties of the particles are accurately modeled, along with the geometry, boundary conditions, and loading conditions of the system. Once the DEM simulation sufficiently resembles the macro-scale physical test results, the data recorded from the DEM simulation can be used to gain further information

about the micromechanical behavior and particle-scale response. To date, there are few if any documented experimentally validated three-dimensional numerical studies which replicate laminar simple shear conditions. This paper presents a study in which experimental data for monotonic DSS element tests on steel spheres were used to validate DEM model simulations. Using DEM simulations of the physical element test to study the microscopic response not only allows for improved understanding of the fundamental mechanisms driving granular material response, they also provide the ability to better understand the DSS device itself.

2. Overview of experiments and simulations

As discussed by O'Sullivan (2014), granular assemblies are highly indeterminate systems, and DEM models can only be analytically validated for unrealistic scenarios involving ideal uniform spherical particles, lattice packings, and relatively simple deformation scenarios. For experimental validation, the physical properties of the material must be known. Steel spheres with high manufacturing tolerances and known material properties have been used successfully in previous validation studies (O'Sullivan et al., 2004; Cui and O'Sullivan, 2006), and they do not suffer from the geometrical variations that are common in glass ballotini, highlighted by Cavaretta et al. (2012). Additionally, these steel spheres are not susceptible to particle crushing, do not exhibit measurable compressible behavior at the range of stresses tested, and they have relatively uniform surface characteristics. This study used American Iron and Steel Institute (AISI) 52100 Grade 25 precision chrome steel spheres manufactured by Thompson Precision Ball. Because of the tendency of uniform sized spheres to crystallize (i.e., form regular packings), three different diameters of spheres were used in each of two test sample configurations (Table 1). The particle diameters were chosen based on the available ball bearings and to keep the particle

sizes in the two samples proportional to each other. Using the two different sets of particle sizes allowed for sample size effects to be explored. The ratios of sample height to the maximum particle diameter were approximately 8 and 15 for sample configurations 1 and 2, respectively. ASTM D6528 specifies that the specimen height shall be greater than 10 times the maximum particle diameter. Sample configuration 1 violated this requirement; however, it was chosen to represent what was thought to be a reasonable lower bound to the number of particles that could be considered in the validation study.

The laboratory and numerical specimens were cylindrical in shape with a diameter of 101.6 mm and a height of approximately 28 mm. This diameter-to-height ratio agrees with recommendations by Franke et al. (1979) and is well within the ASTM D6528 requirements. The experimental sample was confined by a rubber membrane within a stack of approximately 35 thin rings with a low friction coating. To avoid slippage or rolling of the spheres along the top and bottom caps and to ensure shear was transmitted throughout the sample, particles were attached to the top and bottom porous stones using epoxy. This created a rough fixed-particle boundary that was easily modeled in the DEM simulations by setting the velocity of the particles contacting the top and bottom cap equal to that of the contacting cap and setting their rotations to zero. This study used a NGI-type multi-directional direct simple shear device (Fig. 1), and although only monotonic tests were conducted, the device is capable of loading in three independent directions (Rutherford, 2012). The laboratory samples were prepared using air pluviation at three different densities. Variations in the drop height and the flow rate did not achieve noticeable variations in the sample densities. Dense samples were instead created by alternating pluviation and vibration in three layers. For the loose samples, a cylinder with an attached mesh sieve was placed in the bottom of the sample mold. The spheres were pluviated into the mold and the sieve was gently lifted up through the sample.

Once prepared, each sample was tested at a specified stress condition (Table 2). The tests are labeled according to the density ('D' – dense, 'M' – medium dense, and 'L' – loose), vertical stress in kPa, and the sample configuration number. For example, D-50-1 represents a test conducted on a dense sample containing 7,500 particles at 50 kPa vertical effective stress. Because of the large diameter to height ratio, even very small changes in height resulted in substantial deviations in void ratio. This became even more important because the overall range of laboratory void ratios obtainable for the smooth spheres was very low (e.g., void ratio=0.59-0.72 for sample configuration 1). The densest state provided the most reproducible samples and therefore, eight tests were conducted to examine the experimental scatter expected for sample configuration 1. This also gave an indication as to the range of acceptable results for the numerical simulations. Only three similar tests were repeated for sample configuration 2 because the experimental scatter was much lower. Two tests were conducted for each additional density and stress combination; however, only one test was conducted in some cases where the data was used simply for a generic comparison.

The numerical model was created using the PFC3D platform by Itasca Consulting Group, Inc. (Itasca, 2008) to closely match the physical model. The particle sizes and the sample dimensions were identical; however, only 10 confining rings were modeled for most of the simulations. As discussed below, additional simulations with 35 thin confining rings were also developed as part of a parametric study to examine the influence of the ring thickness on the results. All of the material input values used were either provided by the manufacturer, or were directly measured. A simplified Hertz-Mindlin contact model was used in the simulations and the values for shear modulus and Poisson's ratio were chosen based on the manufacturer's material specifications. The inter-particle friction value was experimentally determined using an apparatus described in Cavarretta et al. (2011). An average inter-particle friction angle (ϕ_p) of 5.5 degrees was used based on the range of

determined values. This value agrees with the friction values reported by O'Sullivan (2002). Tilt tests were used to determine the friction values for the ball-wall interface values. Table 3 gives the parameters used in the DEM model.

The DEM samples were initially generated as a non-contacting cloud of spheres and then allowed to settle under gravity into the stack of virtual lateral confining rings, closely replicating the method of air pluviation used in the laboratory. Bernhardt et al. (2012) and (2014) describe extensive parametric studies which assessed the influence parameters such as drop height, wall friction, and inter-particle friction had on the initial void ratio. Because of the computational time required to simulate tamping or vibrating the DEM samples, the densest sample was generated by lowering inter-particle friction, ϕ_p, to 0.5 degrees after pluviation to allow the particles to settle further into place and attain packing densities close to the experimental values. This low friction value was maintained while a top wall, which modelled the top cap in the experimental setup, was inserted and a servo-control algorithm was used to adjust the position of this top wall and attain the experimental stress levels. Once the target stress was attained, ϕ_p was then set back to the actual measured value of 5.5^o before shearing. The use of a low friction coefficient or no friction to create dense samples in DEM analyses has previously been documented by Thornton (2000), Potyondy and Cundall (2004), and Huang et al (2014). Similarly, to produce a loose sample in DEM that matched the laboratory void ratio, ϕ_p was increased to 45^o during gravity settling. Just before the top wall was placed, ϕ_p was set to 5.5^o and maintained at this level while the target stress state was being attained and during shearing. Then the particles in contact with the top and bottom walls were specified to move with the boundaries to replicate the layer of glued particles in the laboratory. Fig. 2(a) shows the laminar boundary walls modeled to represent the stack of confining rings and Fig. 2(b) shows highlights the fixed-particle along the top and bottom boundaries. The bottom wall was specified to move at a constant velocity while the top cap

maintained a constant stress using a servo-control algorithm. These simulations were conducted at velocities that were sufficiently small to ensure quasi-static conditions. The experimental tests were conducted at a common monotonic shear strain testing rate of 5 %/hr which was also shown to be quasi-static (slower shearing rates did not show major changes in the stress-strain curves). The DEM simulation datasets use the same testing designation described above for the experimental results, with the DEM label added. To facilitate direct comparison, the simulations recorded the same type of boundary measurements as in the experiments (i.e., normal stress on the top cap, shear stress on the bottom cap, and vertical movement of top cap).

3. Macro-scale comparison

3.1 Stress-strain and volumetric response

For sample configuration 1, a number of experimental tests were conducted at a vertical effective stress of 50 kPa to establish the repeatability of the results. Fig. 3 illustrates representative test data for the dense and loose samples. The dense samples exhibited a large amount of experimental scatter demonstrated by the fact that the looser of these samples (e_0=0.61) exhibits the highest peak stress ratio. In comparison with the loose samples, the peak stress response of the dense samples is more sensitive to small variations in packing density. The volumetric response of the experimental data, however, is as expected with the denser samples exhibiting more dilative behavior. The extent of the experimental scatter for the dense samples in particular is highlighted to indicate that an exact match with the DEM simulation results cannot be expected, as the material response seems to be highly sensitive to the random variations in packing which will inevitably occur during sample preparation. Also, the spikes or fluctuations in both response data indicate that the number of particles is small and that the overall behavior is sensitive to the collapse of individual strong force chains.

The results from the DEM simulations at two different inter-particle friction values are overlaid onto the experimental data. It is clear that the stress ratio response and the volumetric response are influenced by the inter-particle friction. The observed response for the simulations follows what would be expected; the denser samples have a higher peak stress ratio, and are noticeably more dilative. In comparison with the experiments, the DEM samples are actually less dense and would be expected to have lower peak stress ratios and be more contractive; however, this is not observed for all samples. Therefore, while the response obtained using the average ϕ_p of 5.5° determined by Cavarretta is in general agreement with the experimental data, attaining an accurate match is complicated by the extent of the experimental scatter.

Experimental tests and numerical simulations conducted at 100 kPa vertical effective stress show similar findings (Fig. 4). Overall, the stress ratio response obtained in the DEM simulations agrees well with the experimental data; however, discrepancies in the volumetric response are still present. In contrast to what is expected, the less dense DEM samples demonstrate more dilative behavior. The loose experimental sample exhibits a contractive volumetric response which was not reflected in the DEM results. In fact, no contractive material response was observed for any of the 7,500 particle DEM simulations.

Irrespective of the confining pressures, the DEM simulations give an extremely stiff response at small strains. In general, the experimental results exhibit a softer initial response and show a more distinct strain hardening behavior at larger strains, particularly at the 50kPa confinement. The differences in stiffness are less pronounced for the loose samples. It is also noted that the dense samples do not exhibit a peak stress ratio and then strain soften as might be expected. This is likely due to the fact that the smooth low-friction spheres tested under the relatively low stress conditions used in this study do not interlock like a more angular sand grain would.

Laboratory test data and DEM simulation results for the sample configuration 2 (60,000 particles) are compared in Fig. 5. The experimental scatter for the sample configuration 2 tests was minimal in comparison with configuration 1. While discrepancies in small strain stiffness and volumetric response for the dense sample remain, the overall agreement of all the DEM and experimental results is much better than observed for configuration 1. The small-strain stiffnesses are relatively close for the loose samples and the only differences seen in the stress ratio responses are due to varying initial void ratios. Both the experimental and numerical data follow the expected trends, where looser samples have a lower peak stress ratio and a more contractive response. The dense samples also exhibit some post-peak strain softening which was not seen in sample configuration 1.

One noticeable discrepancy observed in the configuration 2 data is the ability to capture the contractive volumetric response of the loose DEM sample. This type of response was not achieved in any of the samples for configuration 1, indicating a link between the volumetric behavior and the number of particles in the model. While the dilation rates are similar for the experimental and the DEM data shown in Fig. 5, it is clear that the behavior of the dense sample is not fully captured. Even the densest experimental sample slightly contracts initially before dilating; however, this response is not seen in the corresponding DEM data. It is possible that some portion of this overestimation of stiffness could be caused by the limitations of the simple contact model used; however, it is more likely that it may be caused by the sample preparation techniques used to create the dense sample. More discussion of this discrepancy in stiffness is given in Section 3.2.

Both the physical experiments and the DEM simulations indicate that the observed material response is highly sensitive to the number of particles in the simulations, i.e. the particle size relative to the sample dimensions. While the 60,000 particle samples are at similar relative densities, they exhibit lower peak stress ratios when compared to the 7,500

particle sample results. The volumetric response is also shown to be highly dependent on the number of particles modeled for a given sample size. These macro-scale findings agree with conclusions presented by Huang et al. (2014) for a DEM study on the effects of sample size on response. Keeping the same particle sizes, Huang et al. tested three different sizes of rigid wall cylindrical samples under triaxial shear and showed that both volumetric response, stiffness, and peak stress ratio were influenced by sample size.

Examination of the contact force networks for the two sample configurations show the difference in the force chain networks within the two samples (Fig. 6). In Fig. 6, the contact forces are depicted as lines joining the centroids of contacting particles within a central 6 mm thick slice of the sample in the x-z plane. The configuration 2 sample has a large number of force chains which distribute the forces throughout the sample in a relatively even manner. For sample configuration 1, however, relatively few force chains carry a large majority of the applied force. It is clear from the macro-scale response that one single force chain collapse has a non-negligible influence on the overall material response when the total number of force chains is small. The lower computational cost of the DEM simulations makes it attractive to carry out validation tests using samples with relatively small numbers of particles (<10,000); however, the data presented here indicate that the sensitivity of the material response to small variations in packing complicate the comparison and sufficiently high-quality data can only be gathered for samples which have particle numbers above a given threshold.

3.2 Discussion of stiffness in DEM

Even when large numbers of particles are used, it is clear that some details of the physical experiments are not represented in the simulations. Further examination of possible factors influencing the initial stiffness was conducted by exploring the mechanical

compliance in the experimental device, boundary slippage in the physical specimen, and contact model inputs and limitations.

Equipment compliance was checked by comparing the internal displacement measurements of the bottom assembly with those from an external transducer recording the displacement of the bottom cap of the sample (i.e., the cap which the device is displacing). No significant differences were observed. Experimental tests were also carried out using a flat boundary on the top and bottom cap to determine if the fixed-particle sample boundaries were slipping. The results showed no indication that any initial slippage was occurring.

An additional sensitivity study was also conducted on the stiffness parameters and type of contact model used in the DEM simulations. The values for shear modulus and Poisson's ratio used in the Hertz-Mindlin contact model were based on the manufacturer's material specifications for the steel spheres. The equivalent spring constants for the linear spring contact model were calculated according to the Itasca PFC3D manual and a simulation was carried out using the linear contact model. This response was less stiff than the response using the Hertz-Mindlin model; however, it was still not a significant improvement. A simulation was also conducted using the linear contact model with spring constants specified at an order of magnitude less than the constants calculated based on the Hertzian law. The observed stiffness still differed significantly from the experimental data. As discussed by Cavarretta et al. (2010) and Cavarretta et al. (2012), Hertzian contact models do not account for the deformation of surface asperities which occur at contact initiation. Also, as described in Johnson (1985), the Hertz-Mindlin model does not capture any micro-slip that might occur prior to frictional sliding. Both of these features would lead to a stiffer response, but it is unlikely that the limitations of the simplified Hertz-Mindlin model would result in the magnitude of the discrepancy observed for the dense samples in the current study using smooth precision spheres. For example, O'Donovan et al. (2014) compared experimental

bender element tests on glass ballotini and equivalent DEM simulations and found reasonable agreement of the stiffness values when the simplified Hertz-Mindlin contact model was used.

Additional sensitivity studies considered the influence of the viscous damping parameter, but this parameter did not markedly influence the load-deformation response. The sufficiently low strain rates used to maintain quasi-static conditions resulted in very low particle velocities and therefore, viscous damping had negligible effects on the response.

A more plausible explanation for the discrepancy involves a detailed consideration of the sample preparation techniques used. The loose samples were brought to the initial vertical effective stress at the measured ϕ_p of 5.5 degrees. This allowed for contacts, which would not have slipped at the much higher friction value used in pluviation, to slide and for contacts to rearrange as the servo-control stage brought the sample to the required stress state. Just before shearing 29% of the contacts in this loose sample (L-100-2) were either sliding or within 0.1% of the limiting shear force. The dense samples, however, were brought to the target vertical stress at a ϕ_p of 0.5 degrees and then ϕ_p was raised to 5.5^o just before shearing began. Using this technique, contacts which were sliding or on the cusp of sliding were artificially stabilized as the frictional sliding limit at these contacts was increased, and so the fraction of sliding contacts at the start of shearing was 1.12e-03% for the dense sample (D-100-2). At a shear strain of approximately 0.015%, the loose sample reached a steady condition and the percentage of sliding contacts ranged from 52 to 56 percent for the remainder of the shearing. The dense sample, however, did not reach this same steady state until approximately 0.2% shear strain. While a number of prior geomechanics studies, including the key contributions of Thornton (2000) and Potyondy and Cundall (2004) also refer to use of low or no friction to attain dense packings, the results presented here indicate that the resultant samples will exhibit a non-physical load-deformation response at low strain levels, with an artificially high stiffness.

4. Examination of boundary effects and sample inhomogeneity

Following Huang et al. (2014) the homogeneity of the samples at the initial state and during shearing was examined to gain some understanding of the influence of the particle to sample size ratio on the observed response. Homogeneity was quantified both vertically and radially by dividing the sample into zones which were approximately 5.8 mm thick. Five zones were used in the vertical direction and nine zones were used in the radial direction. The zone thickness was selected to always exceed the largest particle diameter. The same zones were used for both sample configurations to directly compare the relationship between particle size and sample size. As described in detail in Huang et al. (2014) the volumes of the spherical particles intersecting the zone boundaries were calculated so that an accurate void ratio within each zone could be determined. The distributions of void ratios normalized by the overall void ratio for sample configurations 1 and 2 at 0, 5, and 10% shear strain are shown in Figs. 7 and 8 for the medium dense samples. Note that the zones are labeled on Figs. 6 and 7 and the vertical zones are referred to as Z_i (Z_1 at the bottom, Z_5 at the top) while the radial zones are named R_i (R_1 at the center and R_9 at the edge). Table 4 details the void ratios for each of the zones, as well as the unbiased sample variances which (following Jiang et al., 2003) are calculated as:

$$S^2 = \frac{1}{m-1}\sum_{i=1}^{m}(e_i - e_{overall})^2 \quad (1)$$

where m is the total number of zones, e_i is the void ratio within zone i, and $e_{overall}$ is the overall void ratio for the total volume of the sample. Referring to Fig. 7, there are large variations in the vertical void ratio distribution for sample configuration 1 for all strain ranges. The void ratio close to the top boundary (V_5) exceeds the overall void ratio by approximately 28% initially, and by 24% at 10% shear strain. A similar effect is noted in the bottom layer (V_1); however, it is not as loose as the top layer. There is a more uniform distribution in void ratio across the height of the sample in configuration 2 with markedly less

variation between the boundary and central zones of the sample. The calculated variance for sample configuration 1 is approximately 0.01 while the variance for sample configuration 2 is approximately 0.002. In both cases, the variance decreases during shearing.

Fig. 8 illustrates the lateral extent of the inhomogeneity. The void ratios for the radial boundary zone (R_9) in both sample configurations well exceed the overall void ratio at all levels of strain. At 10% shear strain, the R9 zone void ratio for sample configuration 2 is approximately 28% greater than the overall void ratio compared to a difference of 34% for sample configuration 1. Although the outside radial boundary void ratio is similar for the samples, the void ratios of the central zones are much more homogeneous for the sample 2 configuration. The overall calculated variance for the radial zones in sample configuration 1 is approximately double the variance of sample configuration 2. While the radial variance is actually higher than the vertical variance for sample configuration 2, the substantial difference between the two sample configurations is found in the vertical direction, where the variance for sample configuration 1 is more than quadruple that of sample configuration 2. Therefore, it is likely that the packing density in the top vertical boundary and the inhomogeneities across the vertical dimension of the sample play a more important role in terms of influencing the stress-strain and volumetric differences.

Large diameter to height ratios have been shown to limit non-uniformities within simple shear samples, but it also appears that the number of particles represented within the core of the element is just as important. For analog or idealized soils where larger particle sizes are used, the homogeneity of the sample should be checked for different particle numbers or sizes to ensure representative simulation results will be achieved. In the case of a simple shear element where the height of the sample is the limiting dimension, it is critical that a sufficient number of particles be represented across the height of the sample.

5. Sensitivity of response to laminar ring boundary configurations

The computational cost of including the individual rings in the simulations was high because it required execution of a customized user-defined function at regular intervals to update the position of the rings. Therefore, a sensitivity study was conducted to examine the influence of the number of lateral confining rings and the ring wall friction on the macro-scale response (Fig. 9). The medium dense sample configuration 1 data are presented in Fig. 9(a), while the sample configuration 2 data are presented in Fig. 9(b). The sample labels also include an additional designation for the number of rings modeled (10 or 35) with the presence of friction designated by the letter 'F'. Both sets of data indicate that the number of rings included in the model does not have a significant effect on the stress-strain response for either sample. The addition of the wall friction, however, has a more significant influence on the response of both samples, although the influence on sample configuration 2 is less marked. Frictional ring walls resulted in a strain hardening response and a higher peak stress ratio. The void ratio distributions were not noticeably sensitive to the presence of friction.

The influence of both wall friction and the number of rings modelled on the deformed specimen shape was also examined. Fig. 10(a) compares the deformed ring profiles for sample configuration 1 with and without friction for the simulations using 10 rings, while Fig 10(b) considers the simulations using 35 rings. Each line shown represents the displacement of the centroid of the ring from its initial position at increments of shear strain of 1%. It is clear from Fig. 10(a) that inclusion of the friction does not significantly change the ring profile. Therefore, the differences observed for the stress-strain and volumetric responses are not likely due to differences in ring displacements. Referring to Fig. 10(b), it is clear that particles are larger than the thickness of the rings and that the profile is determined by the particle movements, thus explaining the insensitivity of the overall material response to the

number of rings. For sample configuration 2, the ring displacements were very smooth and linear for both the 10 and 35 ring tests, as well as with and without friction.

Similar to the homogeneity study discussed above, the void ratios for the vertical and radial zones and the overall variance were calculated to determine whether or not the inhomogeneity would increase if friction (due to the latex membrane) on the ring walls was included in the model. The variance in the vertical and radial directions increased by approximately 4% at 10% shear strain for sample configuration 1 when wall friction was included; however, no differences were noted for sample configuration 2. While the difference in the measured homogeneity is small, the samples with ring wall friction remained in a more dilative state which could explain the strain-hardening behavior. No significant changes in variance were observed for sample configuration 1 when 35 rings were modeled; however, the variance was reduced by over 30% in the radial direction for the sample configuration 2 without friction and by over 40% when friction was present.

6. Conclusions

DEM simulations of laboratory element tests can provide a wealth of information and aid in developing an improved understanding of soil behavior, but it is important for the simulations to be properly validated with laboratory data. This contribution has considered laboratory simple shear tests on samples of steel balls as well as equivalent DEM simulations. Both the physical experiments and the DEM simulations presented indicate that the observed material response is highly sensitive to the number of particles in the simulations, i.e. the particle size relative to the sample dimensions. The results for the samples with configuration 1 (7,500 particles) were very sensitive to small changes in packing and thus an exact match with the DEM simulation data could not be expected. The DEM results were significantly more stiff than the experimental results, they were more dilative, and they did

not follow the expected stress ratio-density relationships. The deviation from the experimental results also worsened with increasing density. Simulation results for samples with configuration 2 however, consisting of 60,000 particles, agreed well with the experimental results for both the stress ratio and volumetric response and all of the results followed the expected trends, confirming the sample height to particle size requirement specified in ASTM D6528. Increasing the number of particles also appeared to be a key factor in successfully capturing the volumetric response for the numerical samples. Therefore, even for validation studies on element tests where the DEM and experimental results can be directly compared, it is important that both sets of samples are comprised of a large number of particles.

Inhomogeneities and sample boundary effects resulting from too few particles influences both the experimental and numerical results. The inhomogeneities are seen in both the contact force network and the packing density. For simple shear samples where the diameter to height ratio is large, the height becomes the critical sample dimension. Increasing the number of particles greatly improved the homogeneity across the height of the sample. Considering both the void ratio and the topology of the contact force network; these improvements in homogeneity lead to better agreement of the overall stress-strain and volumetric responses. These findings indicate that care must be taken for validation studies to ensure that the ratio of the critical sample dimension to particle diameter is sufficiently large. The vertical and lateral void ratio distributions can be used as a preliminary check to assess sample homogeneity.

Examination of various laminar ring wall conditions showed that the inclusion of friction influenced both the stress-strain and volumetric responses; however, the differences observed in sample configuration 2 were less marked. Frictional ring walls led to a more strain hardening and dilative response, as well as slight increases in the vertical and radial

inhomogeneity for sample configuration 1. Modeling 35 rings had little influence on the overall macro-response; however, the calculated variance in void ratio was greatly reduced in the radial direction for sample configuration 2.

The difference in the initial stiffnesses between the physical tests and DEM simulations for the dense samples is most likely caused by the use of a low ϕ_p during the specimen preparation procedure. The data presented here indicate that this approach may lead to non-physical load-deformation response, including artificially high stiffness values, at low strain levels. It seems that the response is less sensitive at large strain levels indicating that this approach is acceptable when looking at peak strength and critical state behavior. Despite the differences in the initial stiffness, when the overall response is considered, the sample configuration 2 simulations agree well with the corresponding experimental results and are therefore, successfully validated.

Acknowledgments

This material is based upon work supported by the National Science Foundation under Grant No. 0449021 and the Graduate Research Fellowship Program. Any opinions, findings, and conclusions or recommendations expressed in this material are those of the authors and do not necessarily reflect the views of the National Science Foundation. The authors would like to thank Ignazio Cavarretta for his contribution to this research in conducting the inter-particle friction tests. The authors also wish to acknowledge the support provided by the Zachry Department of Civil Engineering.

References

Ai, J., Langston, P.A. and Yu, H.-S., 2014. Discrete element modeling of material non-coaxiality in simple shear flows. Int. J. Numer. Anal. Meth. Geomech., 38, 615-635.

Airey, D., Budhu, M., and Wood, D., 1985. Some aspects of the behaviour of soils in simple shear. Developments in soil mechanics and foundation engineering: Vol. 2: Stress-strain modeling of soils, P. K. In Banerjee and R. Butterfield, eds., Elsevier, London, UK, Chapter 6, 185-213.

Bashir, Y and Goddard, J., 1991. A novel simulation method for the quasi-static mechanics of granular assemblages. J. Rheol., 35(5),849-885.

Bernhardt, M.L., O'Sullivan, C., Biscontin, G., 2012. Macro- and Micro-scale Effects of Pluviation Based Sample Preparation in DEM. Proc. of GeoCongress 2012, Oakland, CA.

Bernhardt, M.L., O'Sullivan, C., Biscontin, G., 2014. Effects of Sample Preparation in DEM." Proc. Of IS-Cambridge Micro- to Macro, Cambridge, UK.

Bjerrum, L. and Landva, A., 1966. Direct simple shear test on a Norwegian quick clay. Géotechnique, 16(1), 1–20.

Budhu, M., 1988. Failure state of a sand in simple shear. Can. Geotech. J., 25, 395–400.

Budhu, M. and Britto, A., 1987. Numerical analysis of soils in simple shear devices. Soils Found., 29(2), 31–41.

Cavarretta, I., Coop, M., & O'Sullivan, C., 2010. The influence of particle characteristics on the behaviour of coarse grained soils. Géotechnique, 60(6), 413–423.

Cavarretta, I., Rocchi, I., and Coop, M. R., 2011. A new interparticle friction apparatus for granular materials. Can. Geotech. J., 48, 1829-1840.

Cavarretta, I., O'Sullivan, C., Ibraim, E., Lings, M., Hamlin, S., Wood, D. M., 2012. Characterization of artificial spherical particles for DEM validation studies. Particuology, 10, 209-220.

Cui, L. and O'Sullivan, C., 2006. Exploring the macro- and micro-scale response of an idealized granular material in the direct shear apparatus. Géotechnique, 56, 455–468.

Dabeet, A., Wijewickreme, D., and Byrne, P. M., 2011. Discrete element modeling of direct simple shear response of granular soils and model validation using laboratory element tests. Proc. 2011 Pan-Am CGS Geotechnical Conference, Canadian Geotechnical Society.

Dounias, G. T. and Potts, D. M., 1993. Numerical analysis of drained direct and simple shear tests. J. of Geotech. Engr., 119 (12), 1870–1891.

Franke, E., Kiekbusch, M., and Schuppener, B., 1979. A new direct simple shear device. Geotech. Testing J., 2(4), 190–199.

Huang, X., Hanley, K., O'Sullivan, C., Kwok, F. C. Y, 2014. Effect of sample size on the response of DEM samples with a realistic grading. Particuology, 15, 107-115, http://dx.doi.org/10.1016/j.partic.2013.07.006

Itasca, 2008. PFC3D 4.0 Particle Flow Code in Three Dimensions, Theory and Implementation Volume. Minneapolis, Minnesota.

Jardine, J. R. and Menkiti, C. O., 1999. The undrained anisotropy of k_0 consolidated sediments. Proc. ECSMGE, Amsterdam, The Netherlands.

Jiang, M. J., Konrad, J. M., & Leroueil, S., 2003. An efficient technique for generating homogeneous specimens for DEM studies. Computers and Geotechnics, 30, 579–597.

Johnson, K.L., 1985. Contact Mechanics, 2nd ed., Cambridge University Press, New York.

Kammerer, A., Wu, J., Riemer, M., Pestana, J., Seed, R., 2004. A new multi-directional direct simple shear testing database. Proc. 13th World Conference on Earthquake Engineering, Vancouver, B.C., Canada.

LaRochelle, P., 1981. Limitations of direct simple shear test devices. Laboratory Shear Strength of Soil, ASTM, STP 740, 653-658.

Malek, A. M., 1987. Cyclic behavior of clay in undrained simple shearing and application to offshore tension piles. Ph.D. thesis, MIT.

O'Donovan, J., Hamlin, S., Marketos, G., O'Sullivan, C., Ibraim, E., Lings, M., Wood, D.M., 2015. Micromechanics of seismic wave propagation in granular materials. Proc. IS-Cambridge Geomechanics from Micro to Macro, Vol. 1, 2014, Soga, K., Kumar, K., Biscontin, G., Kuo, M. (Eds.), CRC Press, 305-310.

O'Sullivan, C., 2014. Advancing Geomechanics using DEM. Proc. IS-Cambridge Geomechanics from Micro to Macro, Vol. 1, 2014, Soga, K., Kumar, K., Biscontin, G., Kuo, M. (Eds.), CRC Press

O'Sullivan, C., 2002. The application of discrete element modeling to finite deformation problems in geomechanics. Ph.D. thesis, U.C. Berkeley.

O'Sullivan, C., Bray, J., and Riemer, M., 2004. An examination of the response of regularly packed specimens of spherical particles using physical tests and discrete element simulations. ASCE J. Eng. Mech., 130(10), 1140-1150.

Potyondy, D.O., Cundall, P.A., 2004. A bonded-particle model for rock. Intl. J. Rock Mech. Min. Sci., 41, 1329-1364.

Randolph, M. F. and Wroth, C. P., 1981. Application of the failure state in undrained simple shear to the shaft capacity of driven piles. Géotechnique, 31(1), 143–157.

Rutherford, C. J., 2012. Development of a multi-directional simple shear testing device for characterization of the cyclic shear response of marine clay. Ph.D. Thesis, Texas A&M University.

Saada, A.S., Fries, G., and Ker, C.C., 1983. An evaluation of laboratory testing techniques in soil mechanics. Soils Found., 23 (2), 98-112.

Saada, A. S. and Townsend, F. C., 1981. Discussion: State of the art: laboratory strength testing of soils. Laboratory shear strength of soil. American Society for Testing and Materials, Baltimore, MD.

Shen, C. K, 2013. A micromechanical investigation of drained simple shear tests on dense sand using discrete element simulations. Ph.D. Thesis, Imperial College London.

Shen, C.-K., O'Sullivan, C., and Jardine, R., 2010. A micromechanical investigation of drained simple shear tests. Proc. of Int. Symp. on Deformation Characteristics of Geomaterials, Seoul, Korea.

Shibuya, S. and Hight, D. W., 1987. A bounding surface for granular materials. Soils Found., 27 (4), 123-136.

Talesnick, M. and Frydman, S., 1991. Simple shear of an undisturbed soft marine class in NGI and torsional shear equipment. Geotech. Test. J., 14 (2), 180 -194.

Thornton, C., 2000. Numerical simulations of deviatoric shear deformation of granular media. *Géotechnique*, 50(1), 43-53.

Vucetic, M., 1981. The influence of height versus diameter ratio on the behaviour of Haga clay in the NGI simple shear device. Report no.56204-9, Norwegian Geotechnical Institute, Oslo, Norway.

Zhuang, X., 1993. Computer simulation and experiments on the quasi-static mechanics and transport properties of granular materials. Ph.D. Thesis, University of California, San Diego.

Table 1
Sample size and particle diameters.

Sample Configuration	Number of Particles	Nominal Diameter (mm)
1	2,500	2.38
	2,500	3.18
	2,500	3.97
2	20,000	1.19
	20,000	1.59
	20,000	1.98

Table 2
Experimental testing program.

Test Designation	Void Ratio	Relative Density	Number of Tests
D-50-1	0.60-0.62	96-86%	8
D-50-2	0.59-0.60	91-83%	3
M-50-1	0.65-0.66	60-64%	2
M-50-2	0.62	62%	1
L-50-1	0.67-0.68	39-46%	2
L-50-2	0.64-0.65	35-43%	2
D-100-1	0.60	96%	1
D-100-2	0.59	97%	2
L-100-1	0.66-0.68	43-58%	2
L-100-2	0.63-0.64	46-50%	2
D-200-1	0.59	97%	1

Table 3
Parameters used in DEM simulations.

Parameter	Value Used
Density (kg/m^3)	7800
Shear modulus (GPa)	80
Poisson's ratio	0.3
Interparticle friction angle (degrees)	5.5
Interface friction angle, latex membrane (degrees)	19.8
Interface friction angle, porous stone (degrees)	23.5

Table 4
Void ratios and unbiased sample variations for representative configuration 1 and 2 samples.

	Sample Configuration 1	Sample Configuration 2

	Shear Strain (%)	0	5	10	0	5	10
	Void Ratio, $e_{overall}$	**0.660**	**0.669**	**0.678**	**0.620**	**0.624**	**0.630**
Vertical Zones	1	0.697	0.705	0.711	0.651	0.655	0.659
	2	0.597	0.608	0.620	0.591	0.595	0.602
	3	0.591	0.602	0.614	0.592	0.596	0.603
	4	0.596	0.609	0.628	0.580	0.585	0.593
	5	0.848	0.844	0.841	0.694	0.694	0.697
	Variance, S^2	0.0099	0.0087	0.0075	0.0019	0.0018	0.0017
Radial Zones	1	0.745	0.799	0.908	0.668	0.722	0.809
	2	0.647	0.652	0.660	0.608	0.611	0.616
	3	0.639	0.647	0.654	0.603	0.607	0.616
	4	0.636	0.648	0.655	0.609	0.611	0.617
	5	0.635	0.645	0.655	0.610	0.614	0.620
	6	0.643	0.639	0.638	0.609	0.612	0.617
	7	0.625	0.631	0.647	0.611	0.614	0.619
	8	0.635	0.659	0.661	0.611	0.617	0.619
	9	0.651	0.656	0.683	0.609	0.600	0.610
	Variance, S^2	0.0013	0.0024	0.0064	0.0004	0.0013	0.0037

+Figure Legends

Fig. 1. Multi-directional simple shear device used in experimental validation study (after Rutherford, 2012).

Fig. 2. (a) Laminar boundary walls representing the stack of confining rings, and (b) fixed particle boundary walls in DEM simulations.

Fig. 3. Sample configuration 1 results at 50 kPa vertical effective stress.

Fig. 4. Sample configuration 1 results at 100 kPa vertical effective stress.

Fig. 5. Sample configuration 2 results at 100 kPa vertical effective stress.

Fig. 6. Contact for network for (a) M-50-1 and (b) M-50-2 at 5% shear strain where the magnitude of the contact force is represented by the line thickness.

Fig. 7. Vertical void ratio distributions of DEM sample configurations 1 and 2 shaded to show the value for the zone normalized by the overall void ratio for the sample. Each layer represents approximately 5.8 mm.

Fig. 8. Radial void ratio distributions of DEM sample configurations 1 and 2 shaded to show the value for the zone normalized by the overall void ratio for the sample at each shearing stage. Each layer represents approximately 5.8 mm.

Fig. 9. Stress ratio response with varying ring wall conditions for (a) M-50-1 and (b) M-50-2.

Fig. 10. Ring profiles for M-50-1 (a) 10 rings with and without friction, and (b) 35 rings without friction.

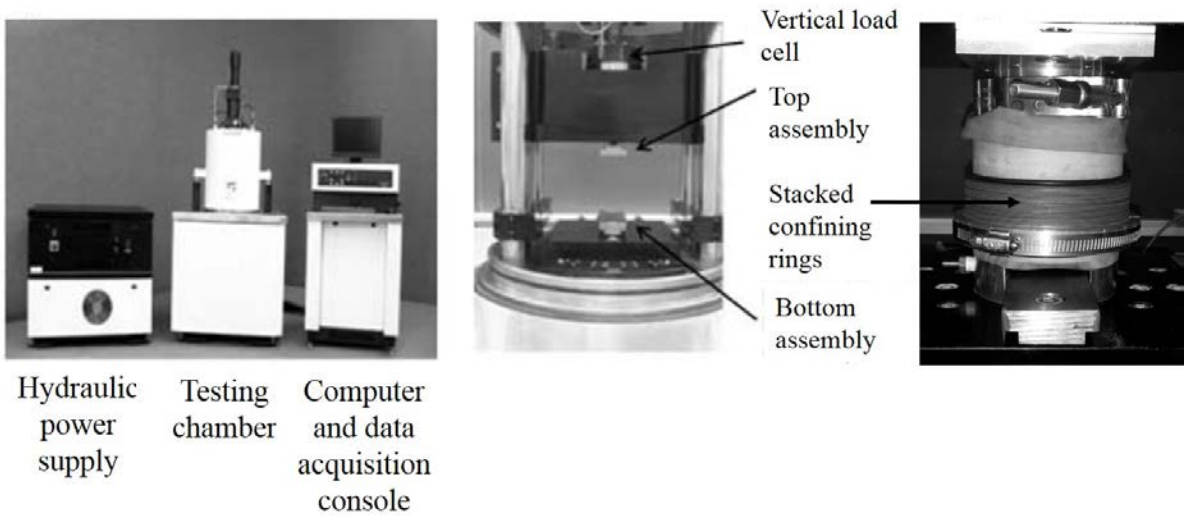

Fig. 1. Multi-directional simple shear device used in experimental validation study (after Rutherford, 2012).

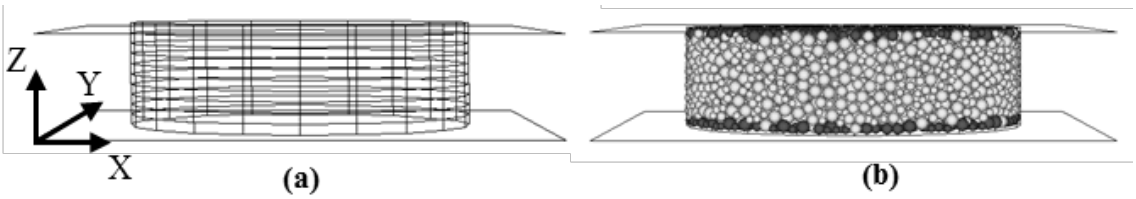

Fig. 2. (a) Laminar boundary walls representing the stack of confining rings, and (b) fixed-particle boundary walls in DEM simulations.

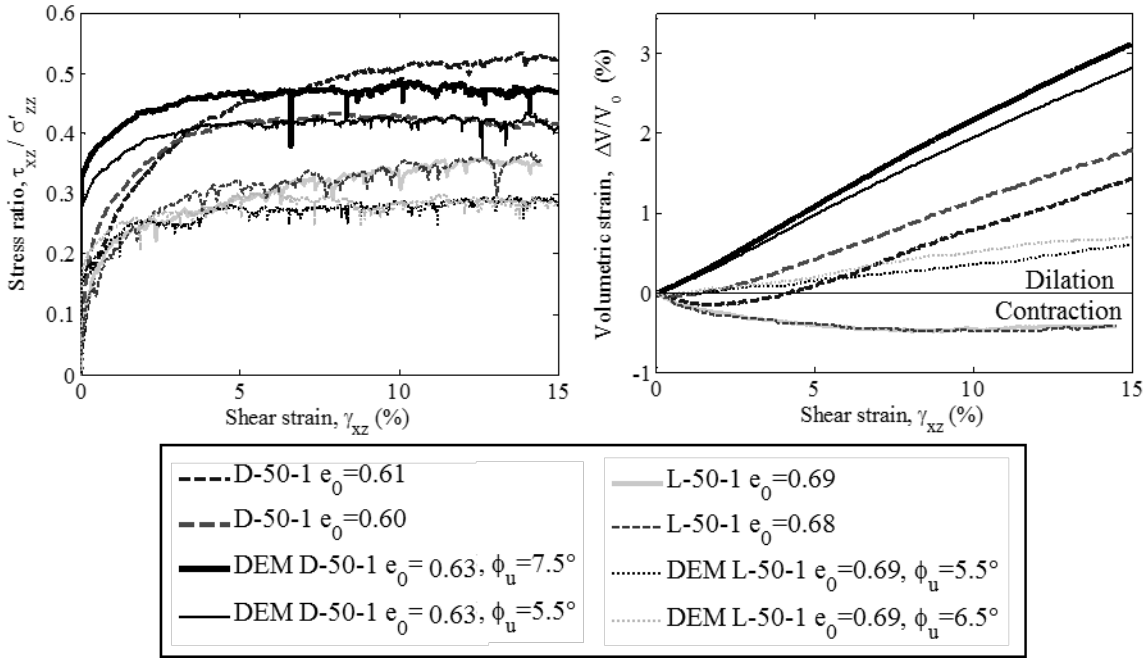

Fig. 3. Sample configuration 1 results at 50 kPa vertical effective stress.

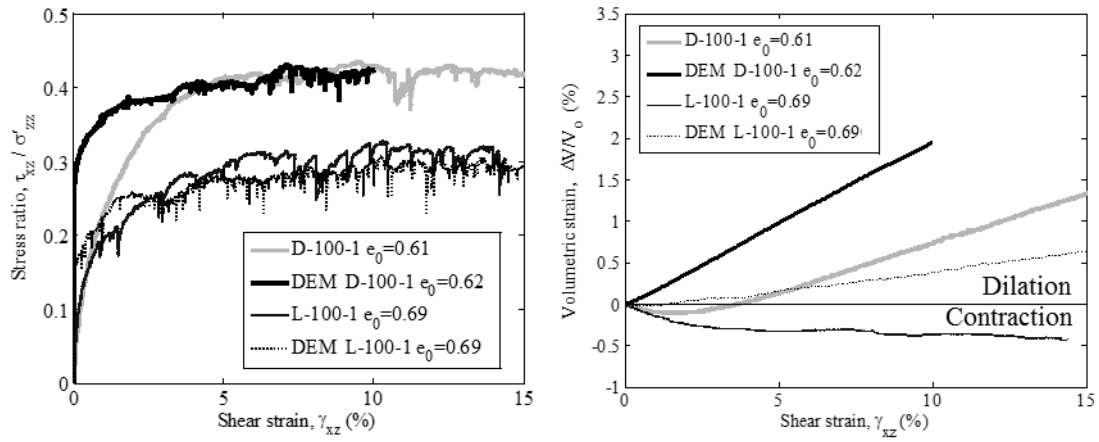

Fig. 4. Sample configuration 1 results at 100 kPa vertical effective stress.

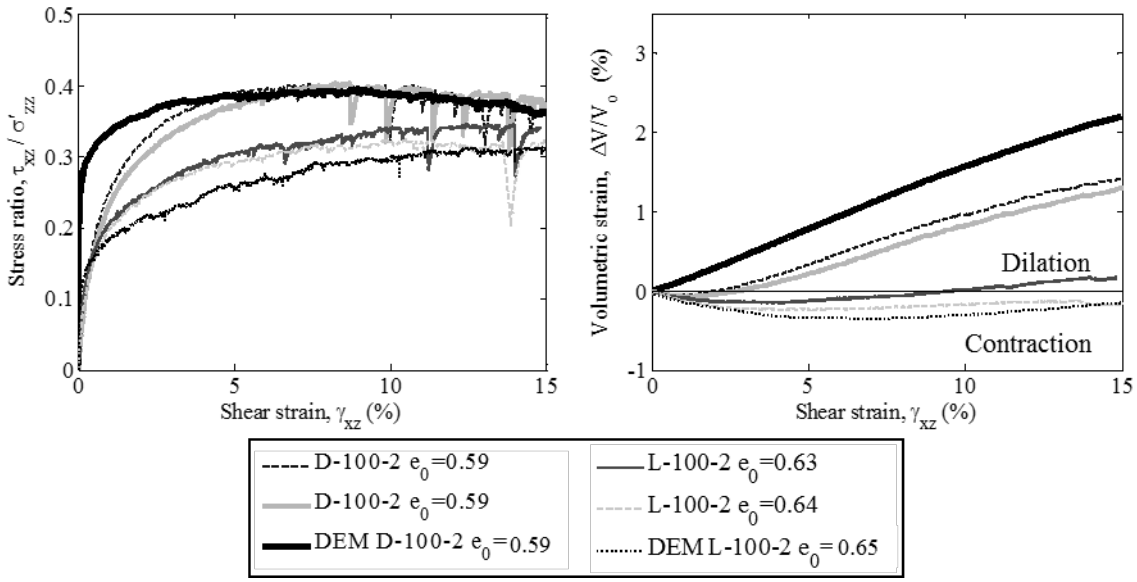

Fig. 5. Sample configuration 2 results at 100 kPa vertical effective stress.

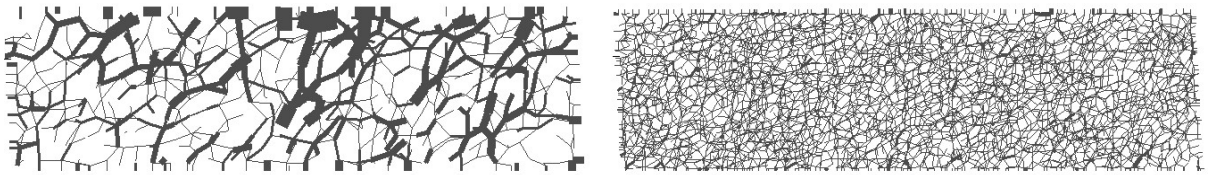

Fig. 6. Contact for network for (a) M-50-1 and (b) M-50-2 at 5% shear strain where the magnitude of the contact force is represented by the line thickness.

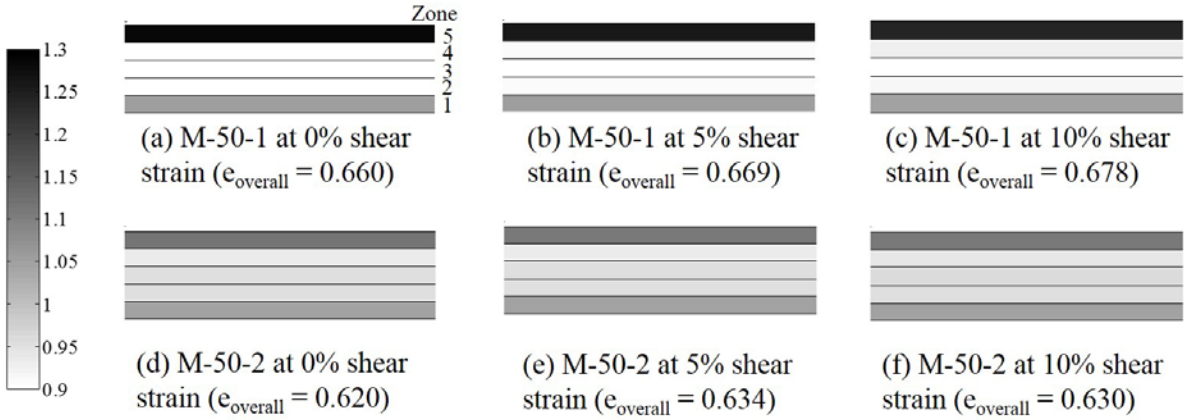

Fig. 7. Vertical void ratio distributions of DEM sample configurations 1 and 2 shaded to show the value for the zone normalized by the overall void ratio for the sample. Each layer represents approximately 5.8 mm.

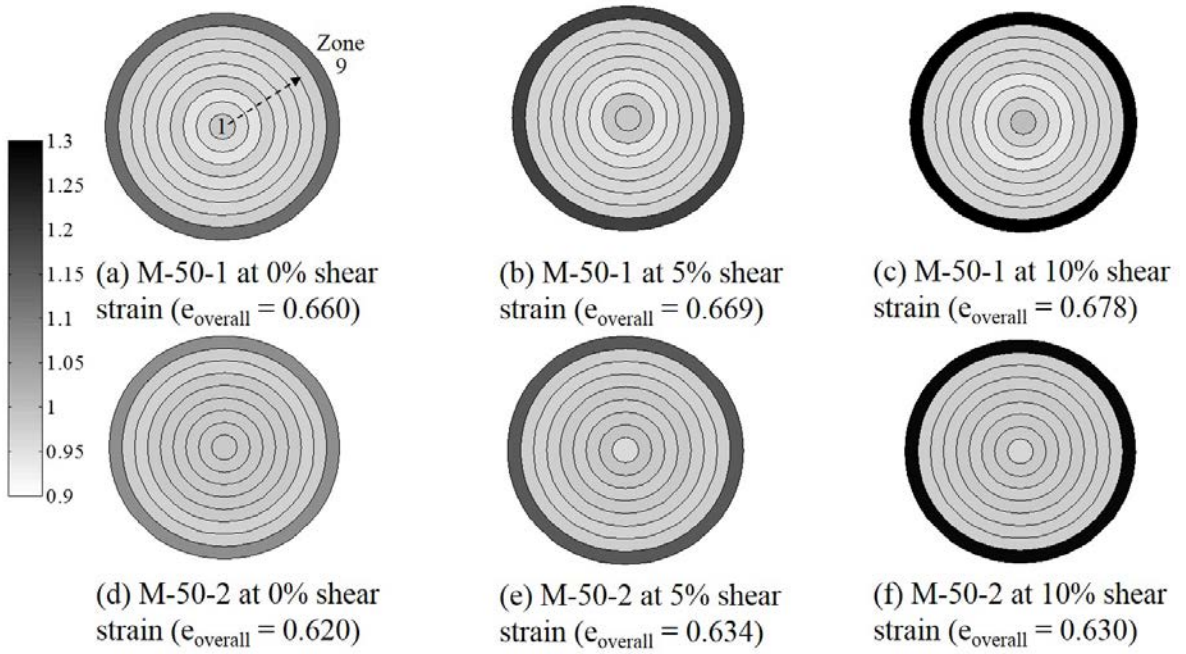

Fig. 8. Radial void ratio distributions of DEM sample configurations 1 and 2 shaded to show the value for the zone normalized by the overall void ratio for the sample at each shearing stage. Each layer represents approximately 5.8 mm.

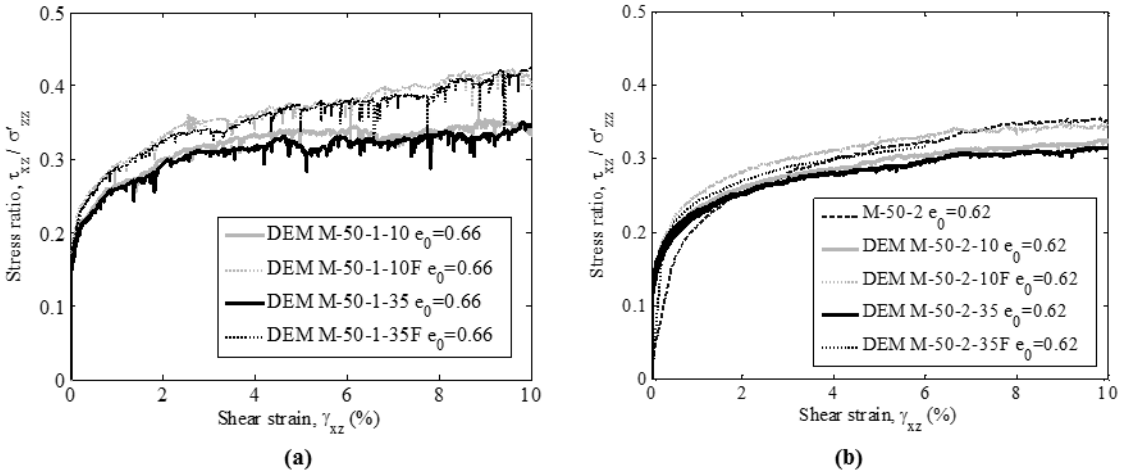

Fig. 9. Stress ratio response with varying ring wall conditions for (a) M-50-1 and (b) M-50-2.

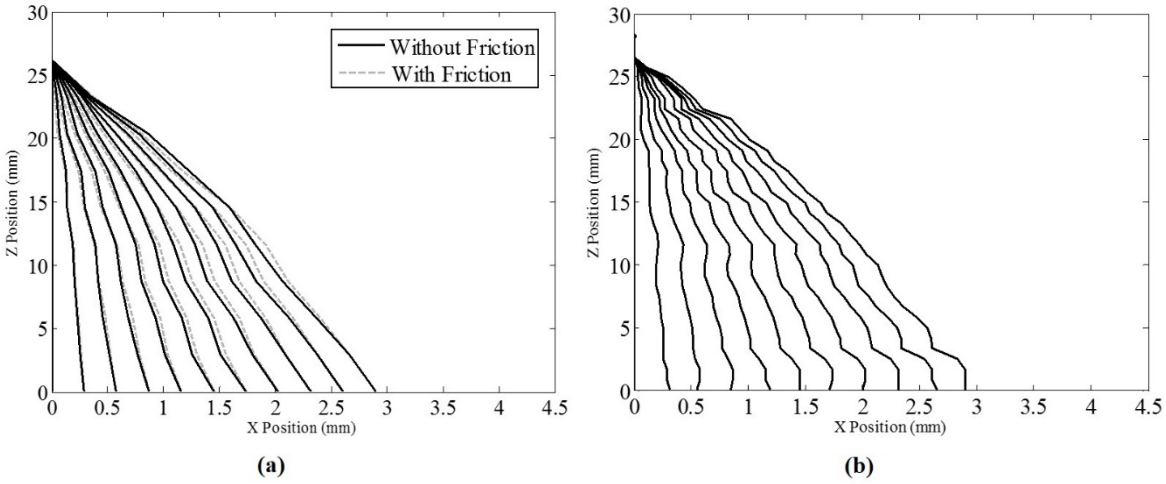

Fig. 10. Ring profiles for M-50-1 (a) 10 rings with and without friction, and (b) 35 rings without friction.